# Aromatic Substrate Specificity of Horseradish Peroxidase C Studied by a Combined Fluorescence Line Narrowing/Energy Minimization Approach: The Effect of Localized Side-Chain Reorganization

M. Laberge, Sz. Osvath, and J. Fidy*

*Institute of Biophysics and Radiation Biology, Semmelweis University, Puskin u. 9, Hungary H-1088*

*Received December 27, 2000*

ABSTRACT: Horseradish peroxidase C binds a wide variety of small H-donor compounds such as benzohydroxamic acid (BHA) and 2-naphthohydroxamic acid (NHA). In this work, we use the Mg(II)-mesoporphyrin prosthetic group derivative as a spectroscopic probe of the active site and of the interaction with the substrates. We report on high-resolution fluorescence line-narrowed spectra which show that the effects of substrate binding on the electronic transitions are similar for both substrates and present data on the normal vibrational modes that are active in the vibronic spectra. Analysis of the vibrational frequencies shows that the Mg(II) ion is 5-coordinate in all cases, thus ruling out a solvent water as sixth ligand. The frequency shifts observed as a result of substrate binding are also indicative of a more rigid prosthetic group upon substrate binding. We present models for MgMP-HRP and its complexes with both substrates and compare the resulting structures on the basis of a modeling approach combining energy minimization to finite difference Poisson−Boltzmann calculations which partitions the various relative protein contributions to substrate binding. We show that the electrostatic potential of the prosthetic group is modified by the binding event. Analysis of the unbound and bound energy-minimized structures shows that the enzyme modulates substrate binding by subtle charge reorganization in the vicinity of the catalytic site and that this rearrangement is not attributable to significant secondary structure conformational changes but to side-chain reorganization.

Horseradish peroxidase (HRP,[1] EC 11.1.7) is an oxidoreductase which catalyzes in plant roots the oxidation of a remarkably wide variety of aromatic compounds by $H_2O_2$ (*1*). Recently, several structures have become available for isoenzyme C: that of native HRPC at 2.15 Å resolution (*2*), as well as the structures of HRPC complexed to BHA (*3*), to ferulic acid and to a ternary cyanide complex at a 2.0 Å resolution (*4*). BHA is not considered a typical HRPC substrate, first of all because it has no known physiological role, although some analogues are reported to be involved in Graminae defense mechanisms (*5*), and second, because it binds more strongly ($K_d = 2.4\ \mu M$) to HRPC than other aromatic substrates which usually have $K_d$s in the millimolar range (*6, 7*). The available X-ray structures are not indicative of any major structural rearrangements as a result of substrate binding, i.e., there is no evidence of clearly distinct structurally "closed" and "open" conformations in the substrate-bound and unbound states: pairwise superposition of the structures yields an overall α-carbon rmsd smaller than 0.4 Å. The X-ray results (*3*) therefore suggest that what makes BHA an atypical reducing substrate is that it has a particular capacity to interact with the active site residues of HRPC, thus confirming earlier reports proposing that aromatic donors bind the enzyme mainly through hydrophobic and H-bonding interactions (*7*−*9*).

In this work, we compare the binding of BHA to that of another similar aromatic donor so as to investigate the details of the aromatic substrate specificity of HRPC and the protein matrix features which control it—and by extension—prosthetic group properties. The other substrate selected was 2-naphthohydroxamic acid (NHA), which also binds HRPC strongly, $K_D$ of 0.2 $\mu$M (*10*), and the binding of which we recently investigated on a fluorescent HRPC derivative by FLN, and also by pressure tuning and Stark effect hole burning spectroscopy (SHB) (*11*, *12*). The structure of the two substrates is shown in Figure 1. In previous studies, we showed that binding NHA increases the Q(0,0) splitting of the optical spectra while the isothermal compressibility did not significantly change. Subsequent Stark effect SHB experiments (*12*) were clearly indicative of different pocket fields being experienced at the optical center as a result of NHA binding. The hole splittings resulting from the application of an electric field, and sensitive to charge effects in the vicinity of the prosthetic group, had markedly different patterns in the free and substrate-bound enzyme.

These results accordingly prompted us to probe the electrostatic environment of the binding site for the NHA complex and also for the BHA complex as previously done in a comparative study on three different peroxidases (*13*) and on *c*-type cytochromes (*14*) using a finite difference

* To whom correspondence should be addressed. Phone: (36-1) 266-2755, ext. 4052. Fax: (36-1) 266-6656. E-mail: judit@puskin.sote.hu.

[1] Abbreviations: BHA, benzohydroxamic acid; EM, energy minimization; FDPB, Finite Difference Poisson Boltzmann method; FLN, fluorescence line narrowing; HRPC, horseradish peroxidase isoenzyme C; MgMP, Mg(II) mesoporphyrin; MgMP-HRP, Mg(II) mesoporphyrin horseradish peroxidase isoenzyme C; NHA, 2-naphthohydroxamic acid; PW, phonon wing; RR, resonance Raman; SHB, spectral hole burning; ZPL, zero phonon line.

10.1021/bi002938a CCC: $20.00 
Published on Web 07/12/2001

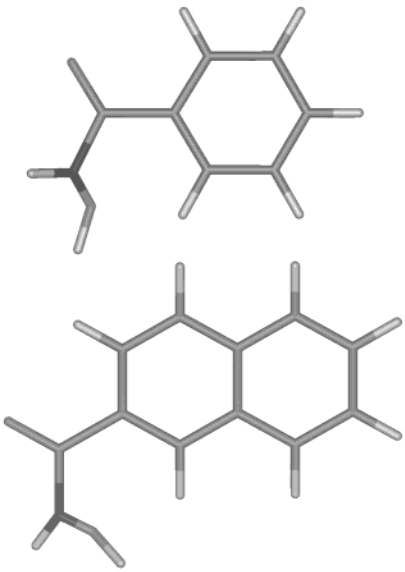

FIGURE 1: Substrates used in the present study: benzohydroxamic acid (top); 2-naphthohydroxamic acid (bottom).

Poisson−Boltzmann (FDPB) approach. The advantage of this method is that it treats the charge−charge interactions explicitely and also accounts implicitely for atomic polarizability and charge reorientation, which are included in the dielectric constant (*15*). In the minimization study, we selected a no cutoff energy minimization approach to locate structurally realistic local minima, a procedure which has been extensively used to investigate structure−function relations in biomolecular assemblies (*16*, *17*), followed by FDPB calculations to generate and compare the electrostatic molecular surfaces of the respective optical centers.

For the experimental FLN measurements, we used the same fluorescent analogue of the native enzyme as in the previous studies as a reporter of the local protein environment, i.e., magnesium mesoporphyrin HRPC (MgMP-HRP), since heme fluorescence is quenched in the native species by the close proximity of porphyrin $\pi^*$ and iron d-orbitals. Interest in this porphyrin derivative is also that it has been the object of reports concerning its cytotoxic activity in the presence of light (*18*).

We have previously used high resolution laser spectroscopy extensively to obtain resolved spectra of porphyrin centers embedded in protein matrixes either by spectral hole burning (SHB) or by FLN and have recently reviewed these techniques as applied to the study of proteins (*19*−*21*). The technique is effective at cryogenic temperatures because the optical centers then behave like impurity hosts in an amorphous glassy matrix. The protein is frozen in a variety of conformational states that lead to a continuous distribution of slightly perturbed electronic transition energies in the optical center. This effect is seen as inhomogeneous broadening in the spectra, the extent of which can be experimentally determined by FLN. The inhomogeneous distribution function (IDF) is the true inhomogeneous (0,0) band shape at low temperature. A typical FLN spectrum is obtained by narrow line width laser excitation within the inhomogeneous absorption band, which then yields line-narrowed emission spectra of the selected population through narrow slit-width detection. The spectral lines of these line-narrowed emission spectra still contain some inhomogeneity due to the spectral

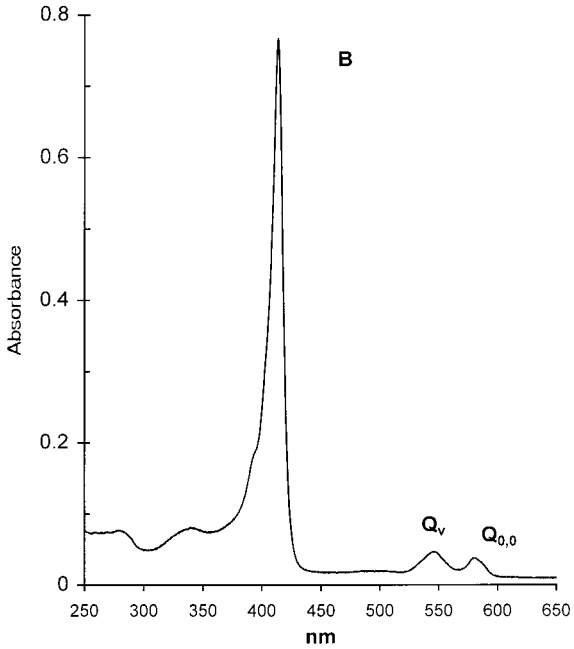


FIGURE 2: Absorption spectrum of MgMP-HRP after liophylization of the main band fractions ($A_{414}$:$A_{280}$ > 9) pooled after G-75 chromatography in 50 mM ammonium acetate, pH 5. Soret (B) at 414 nm, $Q_v$ at 548.0 nm and Q(0,0) at 576.5 nm, $T = 298$ K. The FLN spectra were acquired by tuning the excitation in the Q(0,0) region.

width of exciting laser light and are broadened by the homogeneous line broadening effects (excited-state lifetime, dephasing, temperature broadening, spectral diffusion). The resulting line shape at cryogenic temperatures then consists of a sharp zero phonon line (ZPL) and a broader phonon wing (PW). In the case of optical centers embedded in proteins, coupling of the vibronic transitions to phonon modes of the matrix is also expected (*22*, *23*). The fact that the IDF site symmetries are not significantly different has the result that, selectively exciting a given ZPL transition in the IDF yields emission spectra that only differ by the position of the 0-0 transition without affecting the vibrational features.

The electronic properties of the porphyrin macrocycle (*24*) are based on the well-known four-orbital model which describes the transitions observed in the visible region as occurring between the two highest occupied molecular orbitals ($a_{1u}$ and $a_{2u}$) to the two degenerate lowest unoccupied MOs ($e_g$) (*25*). Under idealized $D_{4h}$ symmetry, the $e_g$ orbitals are strictly degenerate, while $a_{1u}$ and $a_{2u}$ are not. The $e_g$ orbitals are subject to strong configuration interaction with the result that two $\pi \rightarrow \pi^*$ transitions are observed in the visible: the intense (allowed) Soret or B(0,0) transition, in which the transition dipoles add up, and the much weaker Q(0,0) transition, in which the transition dipoles nearly cancel out. A third weak band, $Q_v$, at higher energy than the Q(0,0), is assigned to transitions terminating in higher vibrational levels and mixing with B(0,0) (Figure 2). The Q(0,0) transition of HRPC is of special interest to us, we discuss its $Q_{x-y}$ splitting in a recent report (*26*). In the experiments reported in this work, the $Q_x$-region of the split 0−0 band was selected for excitation to complement the previous FLN results obtained under Q(0,1) excitation (*11*). We also wished to elucidate whether the binding of a 6th ligand could be considered as a possible contributing factor in the previously

observed $Q_{x-y}$ splitting and in the spectral differences between NHA-bound and unbound enzyme (*11*, *12*, *26*). The X-ray structure of the uncomplexed native enzyme clearly shows that a water molecule is not close enough for bond formation (3.2 Å), but since this distance shortens to 2.6 Å in the substrate-bound structure, it could very well be indicative of a 6th ligand as proposed by RR studies (*27*, *28*) or of possible interaction between the water and the porphyrin electron cloud (*3*). Elucidation of the coordination number of $Mg^{2+}$ is also of interest in this class of metalloporphyrins, as the metal has been reported to easily bind to solvent polar impurities (*29*). We show in this work that this question can be answered by FLN. We complement the previous NHA binding studies with FLN results on the binding of BHA and use electrostatic calculations to investigate protein matrix fields in the vicinity of the binding site. The computational results strengthen previously reported Stark effect interpretations on the MgMP-HRP complex with NHA and explain the similarity in the effect of the two substrates (*12*). Energy minimization results show that in both cases, side-chain local reorganization and relaxation fine-tune the charge redistribution of the protein matrix so as to allow aromatic substrate steering.

## MATERIALS AND METHODS

*Derivatization of MgMP-HRP and Sample Preparation.* In this work, we used a derivative of the native enzyme, MgMP-HRP. The insertion of a mesoporphyrin, instead of a protoporphyrin, has been shown to have no effect on the enzyme activity or the formation of the catalytic intermediates, i.e., compounds I, II, and III (*30*) and we have recently reported that our modified MgMP derivatization procedure also has little effect on the substrate-binding properties of the enzyme (*12*), we accordingly fully describe it here.

Horseradish peroxidase isoenzyme C was isolated and purified from horseradish. The heme was removed from the enzyme using the acid methyl ketone method (*31*). The enzyme was then reconstituted with incorporation of the disodium salt of Mg(II) Mesoporphyrin IX (Porphyrin Products, Logan UT). In a typical procedure, some 30 mg of apoHRP were dissolved in 10 mL of 100 mM Tris/HCl buffer, pH 8.2. The mesoporphyrin solution was prepared by dissolving some 3−4 mg of the salt in 1 mL of ethanol (Merck, spec grade) and stirring in the dark for ∼2 h, followed by bench microcentrifugation to remove undissolved material. Some 900 μL of this solution were added to the apoprotein solution; typical concentrations were ∼75 μM MgMP in 50−60 μM apoHRPC. The incorporation proceeded in the dark at 4° C for 2 h. This solution was then dialyzed against two changes of 5 mM KPi, pH 7.0, overnight. The 10 mL dialysate was then centrifuged at 5000 rpm for 1 h at 4° C using Centricon-10000 vials to a volume of 0.5 mL, to remove low molecular weight protein fragments, or alternatively filtered using an Amicon stirred cell with Y10000 membranes (Millipore Corp., Bedford, MA). The concentrate was then applied to a G-75 column (Sephadex Superfine, Pharmacia Fine Chemicals, Uppsala, Sweden), degassed after swelling, bed volume: 76 mL) equilibrated in 20 mM KPi, pH 7.0 and eluted at a rate of 6 mL $h^{-1}$. Only the main band fractions with the $A_{414}/A_{280}$ ratio > 9 were retained and lyophilized (Figure 2). The following extinction coefficients, determined in the laboratory, were used for MgMP in ethanol, $\epsilon_{403} = 3 \times 10^5$ $M^{-1}$ $cm^{-1}$, and for MgMP-HRP in 20 mM KPi, pH 7.0, $\epsilon_{414} = 108$ $mM^{-1}$ $cm^{-1}$. For the FLN experiments, ∼400 μM samples were prepared in 50% glycerol/buffer, which ensures good optical quality at cryogenic temperatures. The buffer used was 50 mM ammonium acetate, pH 5.1. BHA and NHA solutions were prepared in distilled water and in 20% methanol/water (v/v), respectively. A small excess of substrate was added to the enzyme for the FLN experiments.

*Spectroscopy: Fluorescence Line Narrowing.* Low-temperature absorption spectra were acquired with a Jobin-Yvon monochromator THR 1000 with holographic grating (Jobin-Yvon, Longjumeau, France) at a resolution of 2 $cm^{-1}$. Broadband excitation spectra were acquired on a FS900CD luminometer (Edinburgh Analytical Instruments, U.K.) equipped with a Xenon lamp. FLN spectra were recorded using a Coherent 899-01 ring dye laser pumped by an Innova 307 Ar ion laser (Coherent Laser Products, Palo Alto, CA) using Rhodamine 590 (Exciton Laser Dyes, Dayton, OH). The output power was attenuated at the sample to 2−5 mW/$cm^2$ with neutral density filters. In our most recent SHB studies on these derivatives (*26*), we established that efficient SHB in the NHA-bound species requires a power density of at least 5 mW/$cm^2$ and a burntime exceeding 13 min when exciting in the 0-0 region. We also reported that SHB was much less efficient in the absence of NHA. We therefore recorded successive FLN spectra at the same excitation wavelength to verify that SHB did not significantly affect the emission spectra during the acquisition time interval.

The spectral width of the laser line was 0.5 $cm^{-1}$. Excitation spectra were recorded by a motor driving the tuning element of the laser. Emission was recorded at 90° and directed to the THR1000 monochromator (linear dispersion: 0.8 nm/mm, 1200 grooves/mm). The detector was a cooled GaAs R943-02 PMT (Hamamatsu Photonics K. K., Japan). Samples were cooled to ∼10K using a closed cycle M22 refrigerating unit (Cryophysics SA, Geneva, Switzerland). In this type of experiment, the resonant 0-0 emission cannot be recorded due to interference from the exciting laser light and short lifetime of the excited state. Emission spectra were accordingly recorded ∼20 $cm^{-1}$ from excitation using a 200 μm-slit-width, which corresponds to a resolution of 1 $cm^{-1}$ at 590 nm.

*Computational Methods: Generating the Models.* All energy minimization calculations were performed using version 2000 of the *InsightII* software package (MSI, San Diego CA) on a Silicon Graphics R-10000 O2 workstation. Two sets of horseradish peroxidase X-ray coordinates were obtained from the Protein Data Bank (*32*), respectively, pdb1atj.ent for HRPC (*2*) and pdb2atj.ent for HRPC bound to BHA (*3*). The structures were first corrected for the disordered and modified regions resulting from the X-ray procedure. From these coordinates, three structures were generated: (i) that of MgMP-HRP by substituting in 1atj the five-coordinate iron ligated to the porphyrin pyrrole nitrogens and to His170 by magnesium; (ii) that of MgMP-HRP bound to BHA, again by substituting iron with magnesium in the 2atj structure, and (iii) that of MgMP-HRP bound to NHA by substituting NHA for BHA in the previous structure using the Builder module of InsightII to build NHA. Atomic charges for BHA, NHA, and MgMP were obtained from restricted HF calculations as described

elsewhere (*33*). HRPC has two 7-coordinate calcium ions, one ligated to the carbonyl or side-chain oxygens of Asp222, Thr171, Ile228, Asp230, Thr225, with the other coordinated to Val46, Gly48, Asp50, Asp43, Ser52, and wat41. Partial charges were obtained for these coordination spheres using models built by extracting the metals and their ligands from the HRPC structure and optimizing to known model cyclic peptide geometry and within the range of known Ca(II)−O bond lengths in proteins (*34*, *35*). Optimal bond distances and atomic charges for the models were obtained following established procedures (*36*) from RHF/6-31G* calculations (*37*) as implemented in the GAMESS program (*38*) until the changes in energy and coordinates was below $10^{-6}$ Hartrees and $10^{-3}$ Bohr or radians.

The structures were parametrized using the esff force field as implemented in *Discover_3* and incorporating the partial charges calculated for both substrates by an electrostatic fitting procedure. X-ray water molecules were retained, i.e., 150 from 1atj and 197 from 2atj, not counting the water coordinated to Ca352. Retaining these waters was required because some of them participate in the H-bond network, especially the waters found in the heme crevice (*2*, *3*). Additionally, to avoid drastic structural changes during the minimization procedure, the structures were solvated in a 5 Å layer of explicit waters (1394 molecules). This is required so as to include the so-called "structural water shell", consisting of some ∼400 $H_2O$ molecules, strongly bound to the protein surface and which has been shown to stabilize the native structure (*39*, *17*). Explicit hydrogens were added using *InsightII*, and the amino acid residues were protonated so as to be consistent with the experimental pH value. The propionic acid side chains were also considered ionized as inferred from recently reported solvent-accessible surface area calculations for the HRPC heme crevice, which yielded 66.4 $Å^2$, with about half this surface found around the propionates (*33*).

We used a multiple-algorithm protocol for energy minimization so as to relax the structures smoothly, thus avoiding drastic deviations from the initial X-ray structures and consisting of an initial steepest descent minimization to remove artifacts introduced by the addition of explicit hydrogens and solvent until the derivatives reached some 10 kcal $mol^{-1}A^{-1}$ with all heavy atoms tethered. This ensured a nearly quadratic potential energy surface and was followed by conjugate gradient minimization using a Polak-Ribière algorithm, with the backbone atoms constrained in a first step followed by progressive removal of the restraint until the last 30 minimization cycles showed energy differences less than ∼0.01 kcal $mol^{-1}$ with derivatives of the order of 0.0001 kcal $mol^{-1}A^{-1}$. These conversion criteria were deemed appropriate to reach local minima allowing comparison of the relative energies of the different structures. A dielectric constant of 2 was selected with no cutoffs for both van der Waals and Coulombic interactions and the stereochemical quality of the models was verified using the PROCHECK program (*40*).

Ramachandran statistics were examined so as to ensure that the minimized structures were consistent with the allowed Ramachandran ranges and the starting HRPC X-ray structures (Figure 3) The generated models showed good overall intramolecular contacts and no residues had disallowed main torsion angles.

Once all structures minimized, both BHA and NHA were then extracted from their respective structures and each merged into an MgMP-HRP structure, because we wished to take protein relaxation into account as a result of substrate binding. The complexes were then reminimized so as to compare the respective energies of the systems as a result of substrate binding. Since no X-ray structure is available for HRPC-NHA, this substrate was inserted in several starting geometries, rotating it in the heme crevice by 30°-increments with vertical and horizontal translations along the heme plane as well. Four lowest energy structures were then compared with unbound HRPC and the BHA-bound species. It is important to bear in mind that energy minimization is a classical molecular mechanics method. It uses an empirical potential energy function and cannot describe quantum mechanical effects, but the calculated minimized energies can be used for meaningful comparison of the relative binding of two different substrates.

*Electrostatic Calculations*. The charge distribution of the Glu, Asp, Arg, and Lys residues was set to be representative of the experimental pH value. Missing hydrogens were added subject to van der Waals constraints. Electrostatic surface potential maps were generated using the Grasp software package (*41*), which includes a Poisson−Boltzmann (PB) solver, essentially a graphical version of the finite difference solutions to the PB equation implemented in the Delphi software package (*41*−*43*). Briefly, the spatial variation of the potential $\Phi$ at position $\mathbf{r}$ is related to the charge distribution $\rho$ and the position-dependent dielectric permittivity $\epsilon$ as follows:

$$\nabla\epsilon(\mathbf{r})\nabla\Phi(\mathrm{r}) = -4\pi\rho(\mathbf{r})/kT \qquad (1)$$

If mobile ions are present in the system, the Poisson equation can be combined with the Boltzmann expression for ion concentration, yielding:

$$\nabla\epsilon(\mathbf{r})\nabla\Phi(\mathbf{r}) - \epsilon\kappa^2\Phi(\mathbf{r}) = -4\pi\rho^{\mathrm{f}}(\mathbf{r})/kT \qquad (2)$$

where the linearized form of the Poisson−Boltzmann equation is sufficient for most protein applications. The term $\kappa^2$ is equal to $1/\lambda^2$ or $8\pi q^2 I/ekT$ where $\lambda$ is the Debye length, $I$ is the ionic strength of the solution, and $\rho^{\mathrm{f}}$ is the fixed charge density. $\Phi$, $\epsilon$, $\kappa$, and $\rho$ are all functions of the vector $\mathbf{r}$. The second term in eq 2 describes the salt effect. Since water molecules are more polarized by an electric field than the protein, the use of two dielectric constants allows for consideration of the solvation effect experienced by polar molecules in an aqueous solution. The derivative of $\epsilon(\mathbf{r})$ in eq 2 is nonzero only when $\epsilon(\mathbf{r})$ varies, representing the "dielectric discontinuity" region between the low dielectric solute (protein) and the high dielectric solvent or "molecular surface". The *Grasp* PB solver uses two 33 cubed grids, one nested within the other. Electrostatic parameters were set as follows: $\epsilon_{\mathrm{inner}} = 2.0$; $\epsilon_{\mathrm{outer}} = 79.0$; water probe radius = 1.4 Å; ionic radius = 2.0 Å; salt concentration = 0.050 M. The question of the appropriate value for the internal dielectric constant used in this type of calculation has been the object of much debate, essentially because it serves the purpose of accounting for nonexplicit responses to an electric field. We selected to use a value of 2 which assumes that the only dielectric response corresponds to electronic polarizability (*44*). This assumption is justified since the X-ray structures

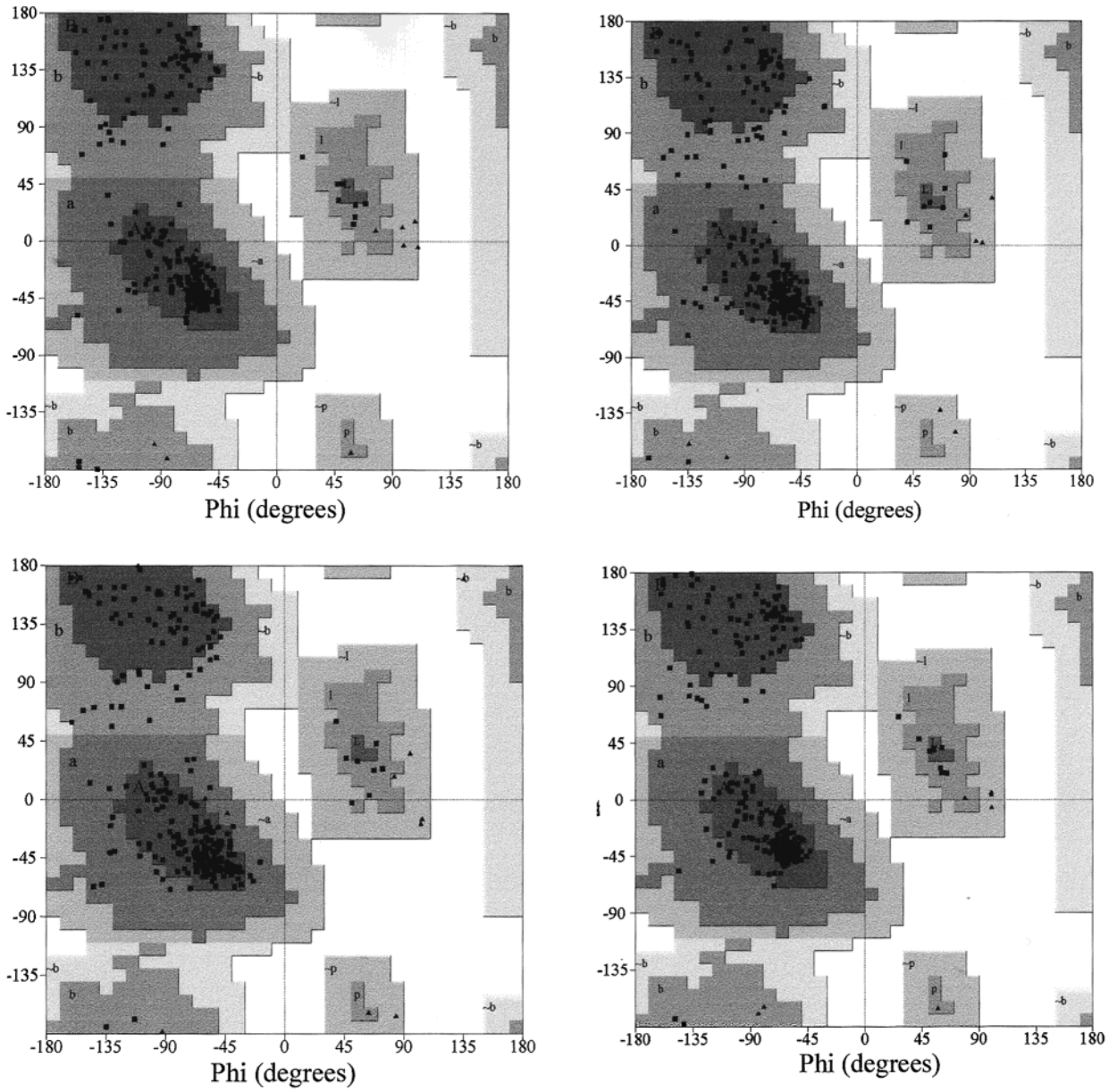


FIGURE 3: Ramachandran diagrams of HRPC structures and models: the top LHS shows the plot obtained for the native HRPC X-ray structure [pdb1atj.ent (*2*)], followed clockwise by the diagrams obtained for (i) the optimized structure of MgMP-HRP, (ii) the X-ray structure of native HRPC bound to BHA [pdb2atj.ent (*3*)], and (iii) the optimized structure of MgMP-HRP bound to NHA.

of the unbound and bound peroxidases are not indicative of major conformational changes in the protein backbone. Calculations were performed using the PARSE (parameters for solvation energy) charge set (*45*) with titratable residues corresponding to their respective pH charge.

## RESULTS

*Low-Temperature Absorption.* Figure 4 shows the absorption spectra of MgMP-HRP (A) and of the enzyme bound to BHA (B) and NHA (C) acquired at 1.5 and 10 K, respectively. The spectra display the Q-band region, observed between ~525 and 600 nm in the 298 K-spectrum which shows $Q_v$ at 541.5 nm and Q(0,0) at 576.5 nm (the latter with $fwhm_{298K} = 13$ nm, cf., Figure 2).

In Figure 4, the $Q_v$ transition clearly displays a spectral envelope indicative of several vibrational transitions (observed between 17 700 and 19 000 $cm^{-1}$). As for the Q(0,0) band, $Q_{x-y}$ splittings of the order of 92, 246, and 255 $cm^{-1}$ are observed for MgMP-HRP, MgMP-HRP/BHA, and MgMP-HRP/NHA. Thus, the effect of BHA is very similar to that of NHA. The sharpness of the bands is also significantly increased at low temperature, with 2nd derivative peak fitting yielding respective fwhm of 43.7, 57.8, and 56.1 $cm^{-1}$ for the lowest energy $Q_x(0,0)$ transitions observed in the spectra of the three derivatives. Previous studies on the protein and on the NHA complex showed good agreement between these spectral width values and the width of the IDF determined by FLN spectral series. Data points for the IDF of the BHA-complex overlaid on the $Q_x$-band illustrates the same for this complex. Note that the IDF is significantly broader for the substrate complexes. The (0,0) region probed by FLN (indicated by arrows in Figure 4) ranges from ~17 000 to ~17 250 $cm^{-1}$.

*Line-Narrowed Spectra*. In condensed phase and if observed at cryogenic temperatures, the PW contribution is known to occur on the high-energy side of the ZPL in

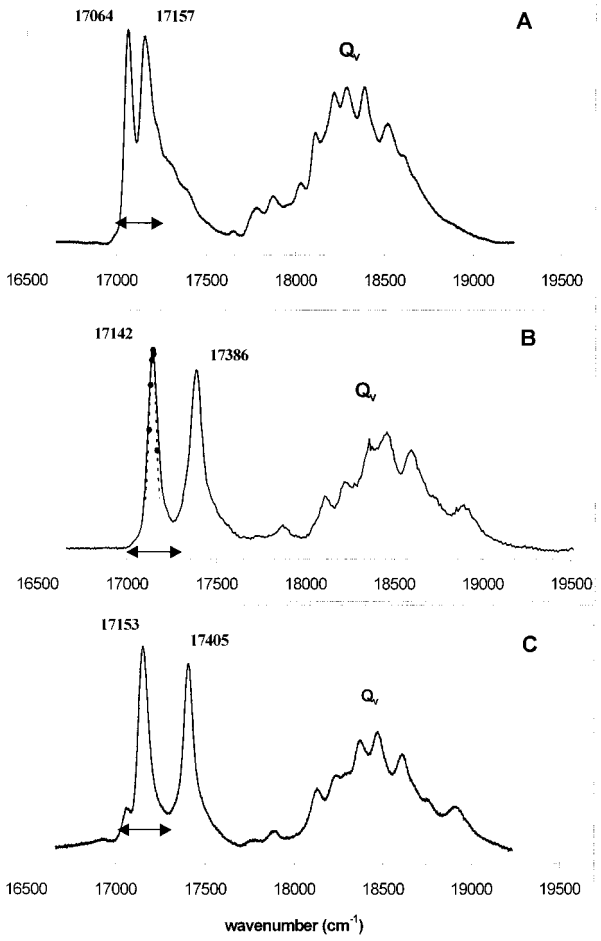


FIGURE 4: (A, C) Absorption spectra of MgMP-HRP and MgMP-HRP/NHA at 1.5 K in the Q-band region; (B) broadband fluorescence excitation spectrum of MgMP-HRP + BHA, same conditions, 10 K. Arrows indicate range of excitation for FLN spectra, namely from 17 021 to 17 245 cm$^{-1}$ for MgMP-HRP and from 17054 to 17304 cm$^{-1}$ for the substrate-bound enzyme. Q(0,0) splittings: MgMP-HRP, 93 cm$^{-1}$; MgMP-HRP + BHA, 244 cm$^{-1}$; MgMP-HRP + NHA, 252 cm$^{-1}$. Dotted line in B: best fit to experimentally determined IDF.

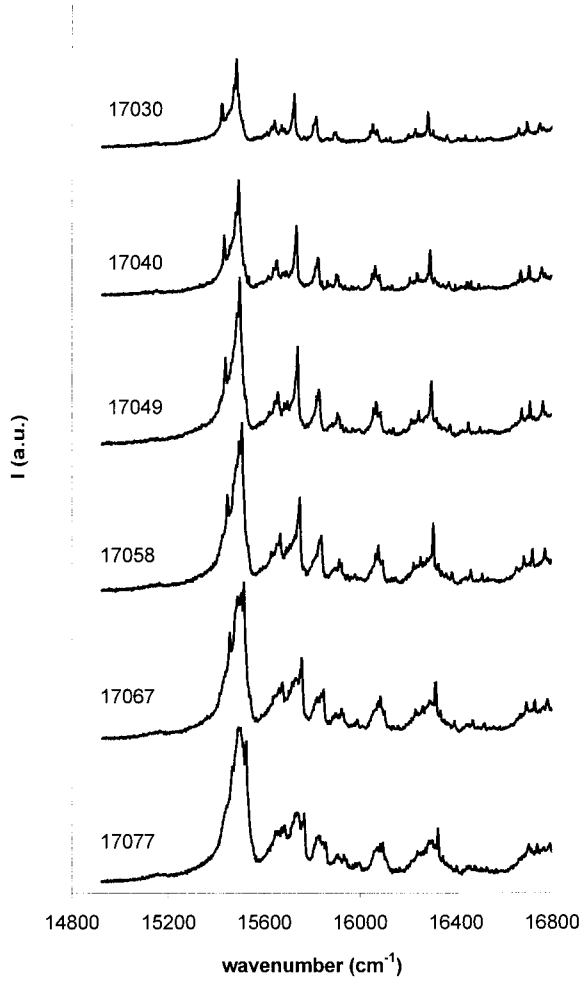


FIGURE 5: FLN spectra of MgMP-HRP in 50 mM AmAc, pH 5.1 and 50% glycerolrecorded by tuning the laser excitation on the low energy side of the $Q_x$ transition at a laser power density of 2−5 mW/cm$^2$. $T = 10$ K, laser excitation wavelength shown on LHS of each spectrum.

absorption and on the low-energy side in emission (*19*, *26*, *46*). Thus, in our experiments, by tuning the laser excitation both to the blue and to the red of the $Q_x(0,0)$ transition, observed at 17 064, 17 142, and 17 153 cm$^{-1}$ in MgMP-HRP, MgMP-HRP/BHA, and MgMP-HRP/NHA, respectively (cf., Figure 4), we are effectively recording the $S_{0,0} \leftarrow S_{1,0}$ transitions of the IDF, with either maximum or minimum contribution from excitation through PW. Figure 5 presents FLN spectra recorded by tuning the excitation on the low-energy side of $Q_x(0,0)$ in the spectrum of MgMP-HRP, i.e., throughout the distribution of 0-0 origins. In the spectrum excited at 17 030 cm$^{-1}$, excitation occurs with the least simultaneous excitation of other oscillators in the inhomogeneous population through their PWs. Another effect is the change in the intensity of sharp lines of ZPL transitions upon tuning the frequency of excitation. This effect is used to determine the IDF of the 0,0 transition (*20*). The most resolved vibronic spectrum with 17 030 cm$^{-1}$ as excitation energy was used to obtain vibrational frequencies for the ground electronic state. These are listed in Table 1 along with comparative data on the symmetry of the active normal modes taken from polarized RR/FLN studies on magnesium−porphyrin complexes (*47*). Differences are observed between the vibrational energies of MgMP in the protein and in its complexed forms. Figure 6 (LHS) shows FLN spectra acquired for MgMP-HRP (A) and for MgMP-HRP bound to BHA (B) and to NHA (C) under identical experimental conditions. The spectra are shown plotted with excitation energy set to zero. Some loss of resolution is observed in the spectra of the substrate-bound enzyme (Figure 6, LHS, panels B and C), that could be attributed to increased PW coupling or to the occurrence of some spectral hole burning during data acquisition. This latter effect cannot be totally excluded, however, if it had been excessive, the lines toward higher vibrational energies would have been more burnt. This is not the case. Possible increased PW coupling with bound substrates was also investigated by recording line narrowed excitation spectra (Figure 6, RHS). In this mode of data acquisition, the burning effect is expected to be minimal, since the experiment is performed by scanning the exciting energy. The emission was monitored through the same vibronic transition in all three cases with the same slit width. It is seen that line narrowing is observed only in the lowest $Q_x(0,0)$ band due to the broadening effect of relaxation in the case of excitation in higher excited-state vibrational levels. The reliability of this experiment is illustrated by

Table 1: Ground-State Vibrations Obtained under 0-0 Excitation for MgMP-HRP and MgMP-HRP Bound to BHA or NHA.

| Mg-HRP | Mg-HRP + BHA | Mg-HRP + NHA | Mg-porphine[a] |
|---|---|---|---|
| ground state | | | |
| 82 w | | | |
| 91 w | | | |
| 148 w | 174 w | 189 w | 185, $A_g$ |
| 166 w | 203 w | | 237 |
| 287 m | 331 w | 336 w | |
| 341 m | 354 m | 359 w | 362, $A_g$ |
| 374 m | 390 w | 399 w | 399, $B_{1g}$ |
| 550 m | 496 w | | 413, $B_{1g}$ |
| 596 m | | | |
| 677 m | 680 w | | |
| 706 w | | | |
| 717 w | | | |
| 733 m | | | 732, $A_g$ |
| 752 m | 755 m | 766 m | |
| 778 w | | | 798, $B_{1g}$ |
| 805 m | 814 w | 822 w | 819, $B_{1g}$ |
| 836 m | | | |
| 870 w | | | |
| 912 w | 922 w | | |
| 964 m | | | |
| 982 m | 982 w | 985 w | 986, $A_g$ |
| 992 m | 996 m | 995 w | 1001, $A_g$ |
| 1059 w | | | 1053, $A_g$ |
| 1080 w | | | |
| 1108 w | | | |
| 1128 w | | | |
| 1134 w | | | |
| 1142 m | 1143 m | 1148 m | 1146, $B_{1g}$ |
| 1221 m | | | 1176, $A_g$ |
| 1231 m | 1234 m | 1242 m | |
| 1311 s | 1312 m | 1320 m | 1326, $B_{1g}$ |
| 1353 w | | | 1342, $B_{1g}$ |
| 1364 w | 1374 w | | 1355, $A_g$ |
| 1392 m | | | |
| 1406 m | 1412 m | 1417 m | |
| 1428 w | | | 1484, $A_g$ |
| 1527 m | | | |
| 1552 s | | | 1559, $B_{1g}$ |
| 1564 m | 1566 m | 1571 m | 1598, $A_g$ |
| 1612 m | 1619 m | 1624 m | |

[a] From ref *47*

comparing the MgMP-HRP absorption and emission spectra (Figure 6a, LHS). The contribution, however, from the $Q_y$ bands of unbound species in the spectra of the samples with substrate (indicated by stars in Figure 6b and c, LHS) unfortunately make it impossible to determine a comparable extent of unresolved background in these cases. The major spectral effect of substrate-binding is to induce both electronic and vibrational lineshifts (cf., Figure 4 and Table 1).

*Energy Minimization: The Minimization Protocol*. Our minimization protocol allowed us to reach local minima which were very close to the starting structures. The minimized MgMP-HRP structures with and without BHA/NHA bound were first compared to the X-ray structures of native HRPC and HRPC + BHA. Ramachandran diagrams (cf., Figure 3) show that the derived models all have good sterically tolerable $\varphi$ and $\psi$ angles. Plots statistics were as follows: HRPC (1atj.ent): 88.5% of the residues in most favored regions and 11.1% in additional allowed regions for a total of 99.6%. A good model is defined as one in which 90% of its residues are found in these regions. The respective analysis for the other structures and models yielded 89.7 and 10.2% for a total of 99.9% for the MgMP-HRP model, 88.2 and 11.4% for a total of 99.2% for the HRPC/BHA 2atj-structure, and 88.2 and 11.4% for a total of 99.6% for the MgMP-HRP/NHA model and 89.0 and 10.8% for a total of 99.8% for the MgMP-HRP/BHA model (diagram not shown). Energy minimization was also attempted in vacuo, but this yielded structures with much higher root-mean-square deviations (rmsd) from the starting structures than the results obtained while retaining the X-ray waters and explicit solvation shell.

*Energy Minimization: The Effect of Substrate Binding*: The effect of substrate binding is summarized in Table 2 which partitions the calculated potential energy differences into contributions from specific interactions to the binding process, i.e., nonbond interactions and the intramolecular strain energies, consisting of all steric and geometric type of interactions according to the form of the potential energy expression. The starting structure for the energy minimization of the substrate-bound enzymes was the same in both cases, i.e., the optimized MgMP-HRP structure into which BHA and NHA were merged in the position which they occupied in the optimized structures of the complexes obtained in the previous modeling and optimization steps. Table 2 reports on one BHA complex and on four complexes with NHA. These are the structures of lowest energy obtained with the EM protocol. Unlike BHA, four different NHA orientations yielded energy minimized structures (NHA to NHA3). Figure 7 shows the superimposed backbones for both BHA and NHA complexes after energy minimization following substrate insertion and Figure 8 plots the rmsd values obtained per residue and the H-bonding pattern emerging as a result of substrate binding is summarized in Table 3.

*FDPB Prosthetic Group Molecular Surfaces*. Figure 9 shows a Grasp rendering of the electrostatic potentials showing the difference in calculated potentials at the prosthetic group molecular surface resulting from the binding of BHA (top) and NHA (bottom). The generated potential surfaces are color-coded with red indicative of a more negative surface and blue, more positive. For BHA, the potential ranges between −39 to 111 mV and for NHA, from −40 to 89 mV. In the case of MgMP-HRP without substrate bound, the potential experienced ranges from −57 to 51 mV (rendering not shown). Thus, the Mg-MPHRP macrocycle feels a more negative potential when substrate is not bound.

## DISCUSSION

*Effect of Substrate Binding on the Normal Modes*. The relationship between resonance fluorescence and resonance Raman (RR) has been discussed elsewhere *(48)*. RR studies on the native enzyme have also shown that native HRPC heme vibrational properties are significantly affected by the presence of BHA (*27*). In this work, the authors showed convincingly how distal heme pocket residues could affect the catalytic mechanism and ligand binding properties of the enzyme. Frequencies determined by FLN for an optical center embedded in a condensed phase such as a protein matrix can be correlated to vibrational normal modes and good agreement with RR data can be reported (*49*).

We discuss first the question of the coordination number of the magnesium. Inspection of the frequencies obtained for all three samples (cf., Table 1) clearly shows that the coordination number of the magnesium atom in our derivative is five. This is based on the observation of three strong

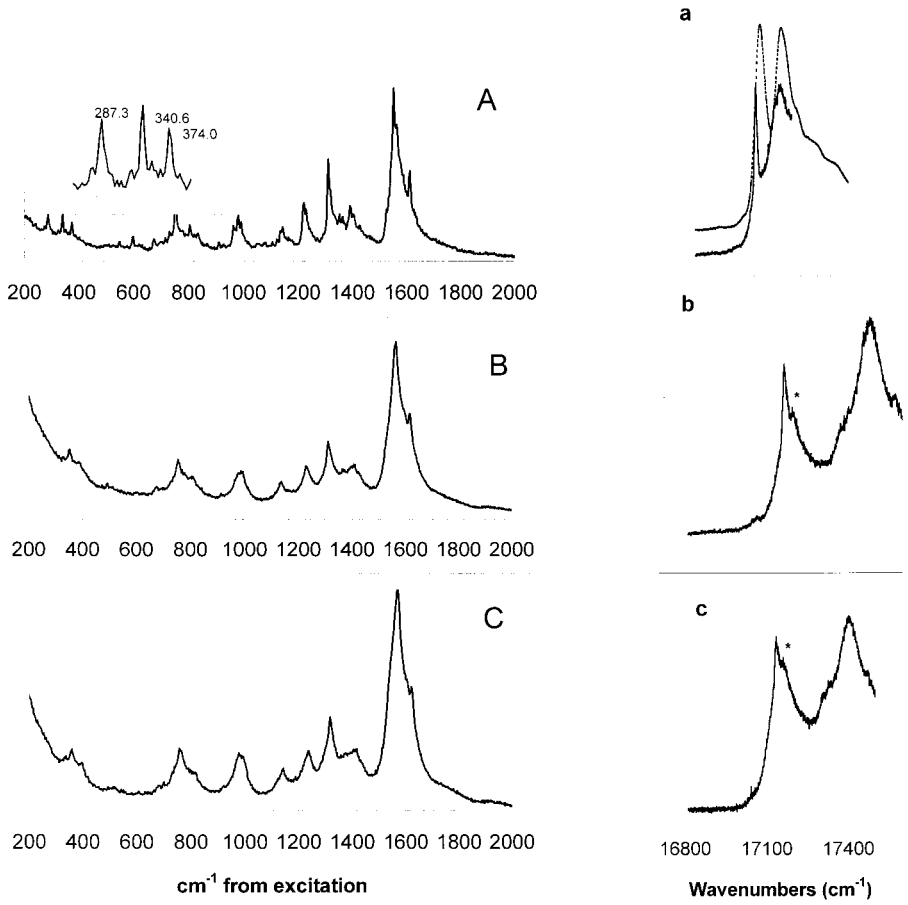


FIGURE 6: (LHS) FLN spectra of MgMP-HRP (A), bound to BHA (B) and to NHA (C) at 10 K; excitation in Q(0,0) band at a laser power density of 2−5 mW/cm$^2$. Spectra are plotted as shift from laser excitation, set at 0 cm$^{-1}$. (Inset) "5th axial-ligand" low-frequency vibrations. (RHS) Laser excitation spectra of (a) MgMP-HRP, (b) MgMP-HRP bound to BHA and, (c) MgMP-HRP bound to NHA. Stars in b and c show bands due to unbound species. The MgMP-HRP excitation spectrum is overlayed with its broadband absorption spectrum (dashed upper overlay). Conditions described in the Materials and Methods, laser power density of 2−5 mW/cm$^2$, $\lambda_{em}$ = 15 748 cm$^{-1}$ for MgMP-HRP and 15 822 cm$^{-1}$ for the substrate-bound derivative, $T$ = 10 K.

bands at 1527, 1552, and 1612 cm$^{-1}$. RR studies on the axial coordination of Mg in chlorophylls *a* and *b* have previously assigned bands at ∼1612−1606 cm$^{-1}$, ∼1554−1551 cm$^{-1}$ (strong), and ∼1529−1527 cm$^{-1}$ to methine bridge stretch modes and correlated them with five-coordinate magnesium (*50*, *51*). This is also in good agreement with the structures obtained from our minimization results showing the metal coordinated to four pyrrole nitrogens and to a fifth ligand, proximal His171. Inspection of the frequencies observed in our spectra show that the coordination of the metal does not increase to six upon substrate binding, as the above-mentioned group of bands do not shift to lower frequency, i.e., to 1599−1596 cm$^{-1}$, 1548−1545 cm$^{-1}$, and to 1521−1518 cm$^{-1}$ as would be expected if the 5-coordinate Mg were to accept an additional axial ligand. Evidence for the 5th axial ligand (His170) comes from a group of frequencies observed in the ∼200−400 cm$^{-1}$ region from excitation. Normal-mode analysis on magnesium-porphyrins has shown that a group of three frequencies observed in the ∼300 cm$^{-1}$ region can be assigned to the vibrations of a fifth axial ligand (*49*). They are clearly seen in our MgMP-HRP spectra (cf., Figure 6, LHS, inset) and still recognizable in the substrate-bound less resolved spectra. It should also be noted that propionate bending modes have been reported as active in this region as well for heme proteins (*52*). The vibration in the ∼750 cm$^{-1}$ region has been assigned in chlorophyll systems to C−C−N and C−N−C types of vibrations (*49*). Table 1 shows that it is sensitive to substrate binding. Another characteristic vibration occurs in the ∼980 cm$^{-1}$ region and is generally assigned to methine vibrations. In our spectra, it is very weak and is not influenced by substrate binding. Overall, the relative intensities of the frequencies listed in Table 1 are not affected by substrate binding but many tend to be upshifted as a *r*esult of binding BHA and NHA with the latter frequencies generally higher than the former. This argues for a more restricted steric environment of the macrocycle in the substrate-bound species.

*Effect of Substrate Binding on the 0-0 Spectral Envelopes.* The MgMP-HRP FLN spectra presented in this work display the effect of the inhomogeneity of the protein matrix upon the vibronic transitions of the MgMP optical center, i.e., the shift of the 0-0 electronic transition energies over ranges that are different for the substrate-bound and unbound derivatives. In the case of the unbound MgMP-HRP, the line width of 43.7 cm$^{-1}$ for the lowest energy Q(0,0) band is in good agreement with the width of the previously determined inhomogeneous distribution function (IDF) of 40 ± 5 cm$^{-1}$ at pH 7.0 (*11*). This function represents the distribution of 0-0 transitions energies. Upon substrate binding, the Q(0,0) extracted from the 10 K absorption spectra and also the IDF broadens to 57.8 and 56.1 cm$^{-1}$ for BHA and NHA, respectively. This could be attributed to an increased

Table 2: Minimization Energy Summary for the Binding of BHA and NHA to MgMP-HRP (four lowest NHA energy structures out of 46 insertion geometries)

| | $E_{initial}$ (kcal mol$^{-1}$) | $E_{final}$ (kcal mol$^{-1}$) | $\Delta E$ |
|---|---|---|---|
| MgMP-HRP + BHA | | | |
| potential, total | −12 483 | −12 946 | 463 |
| internal strain | 1754 | 1643 | 111 |
| nonbond | −14 237 | −14 589 | 352 |
| vdW | −235 | −448 | 213 |
| electrostatic | −14 001 | −14 140 | 150 |
| MgMP-HRP + NHA | | | |
| potential, total | −12 460 | −12 944 | 484 |
| internal strain | 1772 | 1643 | 129 |
| nonbond | −14 233 | −14 587 | 354 |
| vdW | −247 | −436 | 189 |
| electrostatic | −13 985 | −14 151 | 166 |
| MgMP-HRP + NHA1 | | | |
| potential, total | −12 453 | −12 936 | 483 |
| internal strain | 1765 | 1647 | 118 |
| nonbond | −14 218 | −14 583 | 365 |
| vdW | −239 | −441 | 202 |
| electrostatic | −13 979 | −14 143 | 164 |
| MgMP-HRP + NHA2 | | | |
| potential, total | −12 462 | −12 942 | 480 |
| internal strain | 1764 | 1643 | 121 |
| nonbond | −14 226 | −14 586 | 360 |
| vdW | −253 | −417 | 202 |
| electrostatic | −13 973 | −14 168 | 164 |
| MgMP-HRP + NHA3 | | | |
| potential, total | −12 461 | −12 944 | 483 |
| internal strain | 1769 | 1641 | 128 |
| nonbond | −14 230 | −14 585 | 355 |
| vdW | −240 | −421 | 181 |
| electrostatic | −13 990 | −14 164 | 174 |

flexibility of the heme environment as a result of substrate binding, resulting in a broader distribution of transition energies (*53*). It is also possible that the PW contribution is also increased, reflecting stronger electron−phonon coupling upon substrate binding, but experimentally, there remains uncertainty as to the avoidance of concomitant spectral hole burning effects, difficult to avoid when exciting in the 0-0 region.

Another effect of substrate binding is to shift the MgMP-HRP 0-0 origins and to increase the magnitude of the $Q_{x-y}$ splitting as previously reported for NHA (*11*). We observe the same effect with BHA (cf., Figure 4). The 0-0 shift could be indicative of a modified electron density in the $e_g$ ($\pi^*$) orbitals, either induced by porphyrin distortions or by the effect of residues reorganizing charge in the vicinity of the porphyrin optical center, with concomitant modification of van der Waals or electrostatic interactions between the protein matrix and the optical center. Drastic distortions of the porphyrin geometry cannot be the case, as shown by the porphyrin structures extracted from our EM model structures (Figure 10) which reproduce the insignificant structural differences between the hemes in the native HRPC and BHA-bound HRPC X-ray structures (*2*, *3*). This then only leaves the modified electrostatic potential felt at the optical center as a result of binding as clearly shown by their respective electrostatic potential maps (cf., Figure 9). They show an increase of positive potential in the presence of substrate and we propose that this effect could be responsible for the observed 0-0 spectral shifts in the FLN spectra of the substrate-bound enzyme and that it is induced by charge fluctuations in neighboring amino acid residues. It is well-know that the Q-band of porphyrins will shift to higher energy if the electronegativity of the central metal is increased (*54*). Thus, any effect liable to shift electron density away from the ring could account for the significant Q-band shift observed on substrate binding (from 17 064 cm$^{-1}$ in unbound MgMP-HRP to 17142 and 17153 cm$^{-1}$ in the NHA/BHA-bound species, cf., Figure 4). Our potential maps show an increase of negative potential felt at the porphyrin as a result of both BHA and NHA binding (Figure 9). Thus, these calculations, while being in agreement with our most recent Stark effect experiments in that they confirm the experimentally observed charge rearrangement in the heme pocket vicinity following NHA binding (*12*), also predict an increase of negative charge density at the heme which could then account for the observed shift.

As for the increase in $Q_{x-y}$ splitting induced by substrate-binding (*11*), we note that the 246 cm$^{-1}$ observed for BHA are similiar to the splitting previously reported for NHA (255 cm$^{-1}$, ref *11*). Previously, we suggested that this splitting could be attributed to a modified electric field in the heme pocket (*12*, *26*), and the potential maps presented in this work are in agreement with our proposed interpretation. It should be noted, however, that another possible contribution to $Q_{x-y}$ splitting could very well arise from vibronic perturbations, shown to play a significant role in a recent theoretical study on c-type cytochromes (*55*).

*Modeling the Effect of Substrate Binding.* The question now arises as to what factors could be responsible for this charge reorganization when no significant secondary structure conformational change accompanies substrate binding? The EM results (cf., Table 2) are indicative of almost equivalent internal energy contributions to the relaxation energy of the protein as a result of substrate binding. This is in agreement with the X-ray structures reported for the native species which show that the structural effect of binding BHA is limited to a rotation of the ring of Phe68 and to a pocket water molecule moving 6 Å closer to the iron in the case of the substrate-bound structure (*2*, *3*). The binding of BHA is favored over that of NHA by some ∼20 kcalmol$^{-1}$ which is in qualitative agreement with the experimentally determined dissociation constants, the $K_d$ for the binding NHA to MgMP-HRP being ∼10-fold less than that of BHA, i.e., 4 vs 44 $\mu$M, respectively (*12*). A surprising feature of the energy minimization is that different geometries of NHA insertion in the heme pocket yield equally well minimized structures. This points to the great flexibility of the peroxidase in accommodating substrate, and we suggest that this could occur by the modulation of aromatic−aromatic interactions between the rings of Phe residues located at the entrance of the heme edge and the aromatic part of the incoming substrate. We note that the fine details of the aromatic interactions in the vicinity of the substrate do not significantly influence the extent of the electronic energy perturbation felt at the heme: both BHA and NHA binding yield broadened IDFs and the magnitude of their respective $Q_{x-y}$ splitting is also similar. The importance of aromatic interactions has already been recognized (*56*, *57*). Besides Phe68, whose ring rotates to accommodate BHA in the native structure, HRPC presents a unique arrangement of such residues near its catalytic site (namely Phe41, 45, 142, 143, 179, ...). That these rings are capable of reorienting upon substrate binding can be seen in our minimization results. In Figure 8, among

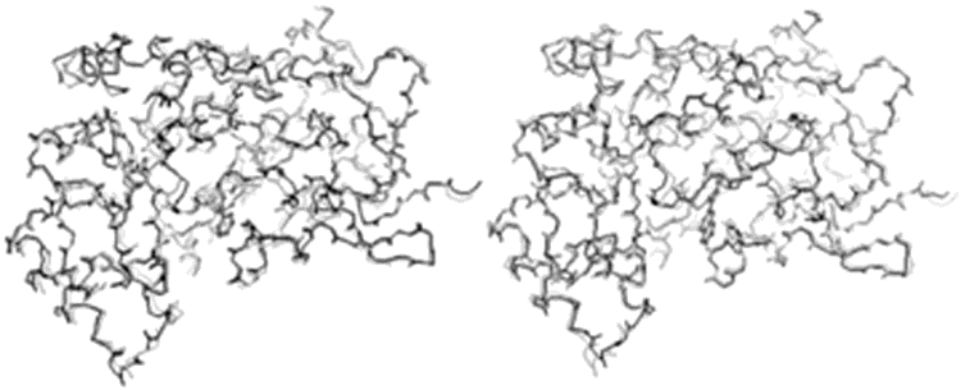

FIGURE 7: Superposed backbone renderings of MgMP-HRP (starting EM structure, gray trace) and of MgMP-HRP + BHA (LHS, black trace) and of MgMP-HRP + NHA (RHS, black trace) after energy minimization following insertion of substrate. For clarity's sake, only one molecule of BHA and NHA shown as a ball-and-stick rendering per superposed pair. Backbone atoms rmsd: 0.15 (BHA) and 0.18 (NHA)

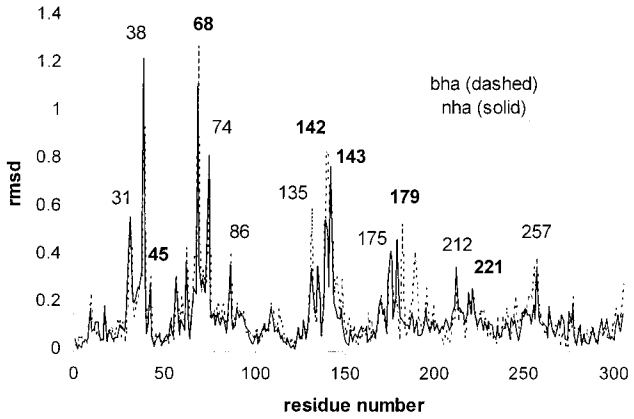


FIGURE 8: rmsd values per residue number for binding of BHA (dashed) and NHA (solid) to MgMP-HRP. Residues with the most significant deviations are labeled by sequence numbers; boldtype: aromatic Phe residues surrounding the heme.

the side chains undergoing the greatest displacements upon substrate binding, we observe most of the Phe groups (boldtype), which are all located near the heme or access channel, including Phe221, on the proximal side of the heme, as well as the significant displacement of Arg38, a long recognized key catalytic residue (*58*, *59*). Theoretically, the nonbond energy is known to represent the major contribution to the minimization of a protein structure (*60*, *61*). This is also supported by our results, in agreement with other computational studies (*62*). Examination of the different protein contributions shows a relatively high internal strain contribution, i.e., some ~23% of the total for BHA and ~26% for NHA, which is somewhat surprising in view of the insignificant change in the secondary structure upon binding, but Figure 8 provides an explanation, i.e., most of that internal strain is due to side-chain rearrangements (rather than backbone torsions or displacements). Aside from the Phe rearrangements, there is concomitant motion of their nearby residues and overall, these rearrangements yield higher rmsd values for the BHA-bound enzyme. The recently published X-ray structure of HRPC bound to ferulic acid (*4*) also shows that the Phe68 ring repositioning is less pronounced when compared to its reorientation in the BHA-bound structure. As NHA, and unlike tight-binding BHA, ferulic acid does not bind the enzyme strongly and the electron density map is suggestive of multiple binding sites. This is paralleled in our energy minimizations which yield several equally optimized structures for the binding of NHA. The aromatic substrate specificity of HRP then appears to be modulated by subtle rearrangements of the enzyme's own aromatic residues. This is reflected in our models by the variation in potentials calculated at the heme (Figure 9), which can then be attributed to R-group local fluctuations and reorganizations which modify in turn the H-bond patterns in the vicinity of the access channel and heme pocket (cf., Table 3). Thus, the more negative potential of the prosthetic group in absence of substrate will stabilize the central positive charge of the macrocycle thus increasing the electron-donating ability of

Table 3: Heme H-Bonds in the MgMP-HRP Minimized Structures with Substrate Bound

| donor | acceptor | distance (Å) |
|---|---|---|
| MgMP-HRP + BHA | | |
| Arg38:HH22 | heme:NA | 2.15 |
| Ser73:HG | heme:O1A | 1.95 |
| Gln176:HE21 | heme:O1A | 2.07 |
| Gln176:HN | heme:O2A | 2.07 |
| Arg31:HE | heme:O1D | 2.24 |
| Ser35:HG | heme:O1D | 1.88 |
| Arg31:HE | hemeO2D: | 1.89 |
| Lys174:HN | heme:O2D | 2.28 |
| Arg38:HH21 | BHA:O1 | 2.07 |
| BHA:HN | Pro139:O | 1.98 |
| heme:NC | W94:O | 2.97 |
| W94:Ho1 | NC | 2.14 |
| W94:HO2 | ND | 2.24 |
| W715:HO2 | heme:O1A | 1.99 |
| W41:HO1 | heme:O1A | 2.11 |
| W52:HO1 | heme:O2A | 2.25 |
| W660:HO1 | heme:O1D | 1.86 |
| MgMP-HRP + NHA | | |
| Arg38:HH22 | heme:NA | 2.35 |
| Arg38:HE | heme:ND | 2.34 |
| Ser73:HG | heme:O1A | 2.01 |
| Gln176:HE21 | heme:O1A | 2.05 |
| Gln176:HN | heme:O2A | 2.00 |
| Gln176:HE21 | heme:O2A | 2.49 |
| Arg31:HE | heme:O1D | 2.07 |
| Arg31:HE22 | heme:O1D | 2.44 |
| Ser35:HG | heme:O1D | 1.94 |
| Arg31:HE | hemeO2D: | 1.92 |
| Lys174:HN | heme:O2D | 2.17 |
| His42:HN | NHA:O1 | 2.07 |
| heme:NC | W94:O | 2.71 |
| W715:H12 | heme:O1A | 2.06 |
| W41:HO1 | heme:O1A | 2.05 |
| W52:HO1 | heme:O2A | 1.89 |
| W660:H11 | heme:O1D | 1.95 |

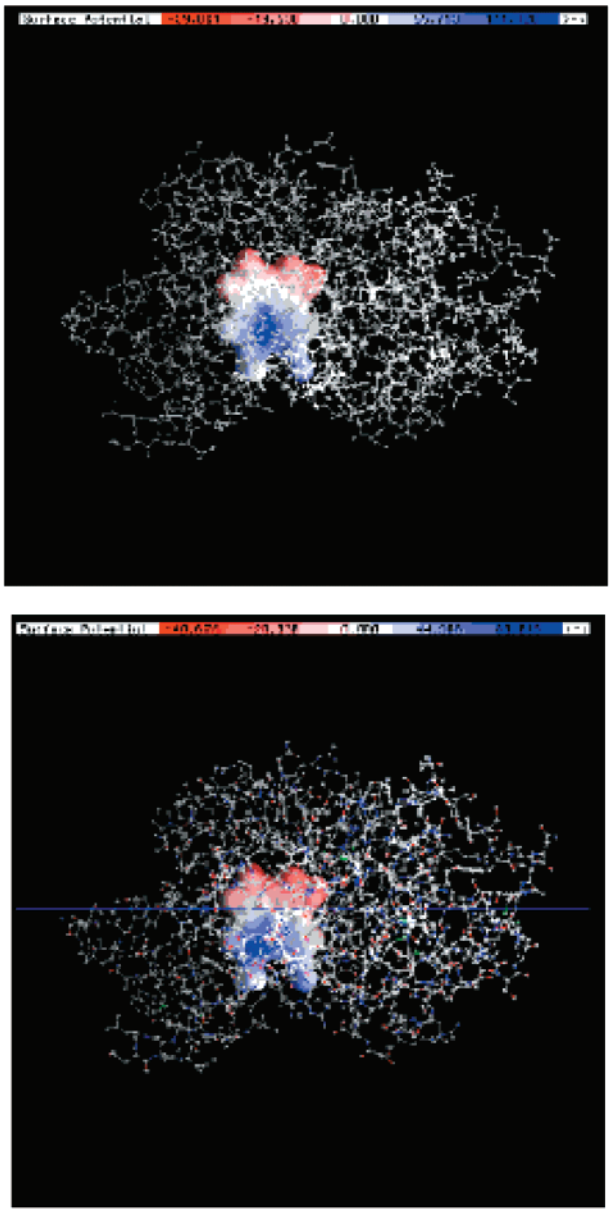

FIGURE 9: Heme electrostatic potentials showing the difference in calculated potentials at the heme molecular surface relating from the binding of BHA (top) and NHA (bottom). The heme potential surfaces are color coded: red, more negative; blue, more positive. For BHA, the potential ranges between −39 to 111 mV and for NHA, from −40 to 89 mV. For the unbound enzyme (not shown), the potential ranges between 57 to + 50.8 mV.

an incoming aromatic substrate. Our results are also in good agreement with a previous report showing that the electrostatic potential imposed by the protein matrix on the heme active site was very different for a series of compared peroxidases and strongly influenced essential peroxidase properties (*13*). They are also in good agreement with our previous pressure tuning and Stark effect experiments which provided experimental evidence for protein charge reorganization near the prosthetic group (*11*, *12*). In our last study (*12*), investigating the role of the central metal in substrate binding, we proposed that HRPC was capable of sampling "electrostatic" rather than "structural" substates. The modeling of the substrate-bound and unbound states of HRPC presented in this work is indicative of electrostatic substate-modulation via localized side-chain fluctuations (*33*, *63*).

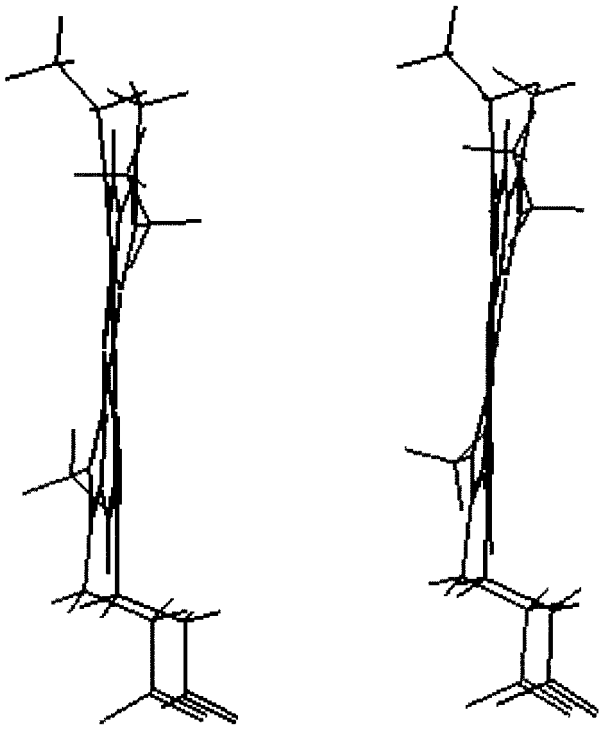

FIGURE 10: Porphyrin prosthetic group extracted from the MgHRP/BHA (LHS) and MgHRP/NHA (RHS) structures.

## CONCLUSIONS

In this study, we compared the binding of two small aromatic substrates to MgMP-HRP. Line-narrowed fluorescence and excitation spectra acquired for both MgMP-HRP and the substrate-bound species yield vibrational frequencies which are increased due to the substrate binding event and show that the Mg ion is 5-coordinate in all samples. Substrate-binding results in a shift of 0-0 origins and increased $Q_{x-y}$ splitting with similar spectral characteristics for the two substrates. Computational modeling shows a modified electrostatic potential felt at the prosthetic group, resulting from localized rearrangements of (mainly) aromatic side chains in its vicinity. These effects are distinct in the case of BHA and NHA binding. Besides being in good agreement with previously reported Stark effect SHB results (*12*), the electrostatic modeling also contributes a methodology to investigate binding events which are not accompanied by significant structural conformational changes, nor by electrostatic complementarity between protein and substrate. Further work, using a recently developed dynamic electrostatic sampling approach investigates the time scale of these R-group fluctuations (*33*, *63*).

## ACKNOWLEDGMENT

The authors thank the Hungarian National Foundation Grants OTKA T-032117 and T-25545 for support. M.L. and S.O. also gratefully acknowledge support from Hungarian Grant MKM FKFP 1191/1997 (J.F.). R. A. Laskowski (UC London, GB) is also gratefully thanked for providing the PROCHECK program. The technical assistance of Mrs. R. Markács in sample purification and preparation is greatly appreciated.

## REFERENCES


1. Dunford, B. H. (1991) in *Peroxidases in Chemistry and Biology* (Everse, I., Everse, K. E., and Grisham, M. B., Eds.) pp 1−24, CRC Press, Boca Raton.
2. Gajhede, M., Schuller, D. J., Henriksen, A., Smith, A. T., and Poulos, T. L. (1997) *Nat. Struct. Biol. 4*, 1032−1038.
3. Henriksen, A., Schuller, D. J., Meno, K., Welinder, K. G., Smith, A. T., and Gajhede, M. (1998) *Biochemistry 37*, 8054−8060.
4. Henriksen, A., Smith, A. T., and Gajhede, M. (1999) *J. Biol. Chem. 274*, 35005−35011.
5. Veitch, N. C. (1995) *Biochem. Soc. Trans. 23*, 232−260.
6. Veitch, N. C. (1995) *Eur. J. Biochem. 229*, 629−640.
7. Paul, K. G., and Ohlsson, P. I. (1978) *Acta Chem. Scand. B32*, 395−404.
8. Schejter, A., Lanit, A., and Epstein, N. (1976) *Arch. Biochem. Biophys. 174*, 36−44.
9. Veitch, N. C., Williams, J. P., Bone, N. M., Burke, J. F., and Smith, T. A. (1995) *Eur. J. Biochem. 233*, 650−658.
10. Schonbaum, G. R. (1973) *J. Biol. Chem. 248*, 502−511.
11. Balog, E., Kis-Petik, K., Fidy, J., Köhler, M., and Friedrich, J. (1997) *Biophys. J. 73*, 397−405.
12. Balog, E., Galantai, R., Koehler, M., Laberge, M., and Fidy, J. (2000) *Eur. Biophys. J. 29*, 429−438.
13. Welinder, K. G., Bjornholm, B., and Dunford, H. B. (1995) *Biochem. Soc. Trans. 23*, 257−262.
14. Laberge, M., Köhler, M., Vanderkooi, J., and Friedrich, J. (1999) *Biophys. J. 77*, 3293−3304.
15. Gunner, M. R., and Honig, B. (1991) *Proc. Nat. Acad. Sci. 88*, 9151−9155.
16. Brooks III, C., Karplus, M., and Montgomery Pettitt, B. (1988) in *Proteins: A Theoretical Prespective of Dynamics, Structure, and Thermodynamics*, Vol. LXXI, Interscience, J. Wiley and Sons, New York.
17. Ma, J., and Karplus, M. (1997) *J. Mol. Biol. 274*, 114−131.
18. Deguchi, J., Tamura, M., and Yamazaki, I. (1985) *J. Biol. Chem. 260*, 15542−15546.
19. Fidy, J., Balog, E., and Koehler, M. (1998) *Biochim. Biophys. Acta 1386*, 289−303.
20. Fidy, J., Laberge, M., Kaposi, A., and Vanderkooi, J. (1998) *Biochim. Biophys. Acta 1386*, 331−351.
21. Köhler M., Friedrich J., Fidy J. (1998) *Biochem. Biophys. Acta 1386*, 255−288.
22. Schlichter, J., Friedrich, J., Herenyi, L., and Fidy, J. (2000) *J. Phys. Chem. 112*, 3045−3050.
23. Osad'ko, I. S. (1983) in *Spectroscopy and Excitation Dynamics of Condensed Molecular Systems* (Agranovich, V. M., and Hochstrasser, R. M., Eds.) pp 437−514, North-Holland, New York.
24. Makinen, M. W., and Churg, A. K. (1983) in *Iron Porphyrins* (Lever, A. B. P., and Gray, H. B., Eds.) pp 141−235, Addison-Wesley, Reading, MA.
25. Gouterman, M. (1978) in *The Porphyrins*, (Dolphin. D., Ed.) pp 1−156, Academic Press, New York.
26. Suisalu, A., Mauring, K., Kikas, J., Herenyi, L., and Fidy, J. (2000) *Biophys. J. 80*, 498−504.
27. Smulevich, G., English, A. M., Mantini, A. R., and Marzocchi, M. P. (1991) *Biochemistry 30*, 772−778.
28. Howes, B. D., Rodriguez-Lopez, J. N., Smith, A. T., and Smulevich, G. (1997) *Biochemistry 36*, 1532−1543.
29. Platenkamp, R. J., and Noort, M. (1982) *Mol. Phys. 45*, 97−112.
30. Hewson, W. D., and Hager, L. P. (1979) in *The Porphyrins* (Dolphin, D., Ed.) pp 295−332, Academic Press, New York.
31. Teale, F. W. J. (1959) *Biochim. Biophys. Acta 35*, 543.
32. Bernstein, F. C., Koetzle, T. F., Williams, G. J. B., Meyer, E. F., Jr., Brice, M. D., Rodgers, J. R., Kennard, O., Shimanouchi, T., and Tasumi, M. (1977) *Eur. J. Biochem. 80*, 319−324.
33. Schay, G., Galantai, R., Laberge, M., and Fidy, J. (2001) *Int. J. Quantum Chem. 84* (in press).
34. Jois, D. S. S., Prasad, G. S., Bednarek, M., Easwaran, K. R. K., and Vijayan, M. (1993) *Int. J. Pept. Protein Res.* 41, 484−491.
35. Frausto da Silva, J. J. R., and Wiliams, R. P. G. (1991) *The Biological Chemistry of the Elements: The inorganic Chemistry of Life*, Clarendon Press, Oxford.
36. Norrby, P.-O., and Liljefors, T. (1998) *J. Comput. Chem. 19*, 1146−1166.
37. Hariharan, P. C. (1973) *Theor. Chim. Acta 28*, 213−222.
38. Schmidt, M. W., Baldridge, K. K., Boatz, J. A., Elbert, S. T., Gordon, M. S., Jensen, J. H., Koseki, S., Matsunaga, N., Nguyen, K. A., Su, S., Windus, T. L., Dupuis, M., and Montgomery, J. A. (1993) *J. Comput. Chem. 14*, 1347−1363.
39. Fujisawa, T., Uraga, T., Yamaizumi, Z., Inoko, Y., Nishimura, S., and Ueki, T. (1994) *J. Biochem. 115*, 875−880.
40. Laskowski, R. A., MacArthur, M. W., Moss, D. S., and Thornton, J. M. (1993) *J. Appl. Crystallogr. 26*, 283−291.
41. Nicholls, A., and Honig, B. (1991) *J. Comput. Chem. 12*, 435−445.
42. Jayaram, B., Sharp, K. A., and Honig, B. (1989) *Biopolymers 28*, 975−993.
43. Nicholls, A., Sharp, K. A., and Honig, B. (1991) *Proteins 11*, 281−296.
44. Sheinerman, F. B., Norel, R., and Honig, B. (2000) *Curr. Opin. Struct. Biol. 10*, 153−159.
45. Sitkoff, D. K., Sharp, K. A., and Honig, B. (1994) *J. Phys. Chem. 98*, 1978−1988.
46. Personov, R. I. (1983) in *Spectroscopy and Excitation Dynamics of Condensed Molecular Systems* (Agranovich, V. M., and Hochstrasser, R. M., Eds.) pp 555−619, North-Holland, New York.
47. Solov′ev K. N., Stanishevskii I. V., Starukin A. S., Shul'ga A. M., Egorova G. D. (1984) *ZhurPrikl. Spekt. 40*, 765−773.
48. Hochstrasser, R. M., and Nyi, C. A. (1979) *J. Chem. Phys. 70*, 1112−1128.
49. Avarmaa, R. A., and Rebane, K. K. (1985) *Spectrochim. Acta 41A*, 1365−1380.
50. Fujiwara, M., and Tasumi, M. (1986) *J. Phys. Chem. 90*, 250−255.
51. Fujiwara, M., and Tasumi, M. (1996) *J. Phys. Chem. 90*, 5646−5650.
52. Feis, A., Marzocchi, M. P., Paoli, M., and Smulevich, G. (1994) *Biochemistry 33*, 4577−4583.
53. Frauenfelder, H., Sligar, S. G., and Wolynes, P. G. (1991) *Science 254*, 1598−1603.
54. Gouterman, M. (1959) *J. Chem. Phys. 30*, 1139−1143, and private communication.
55. Schweitzer-Stenner, R., and Bigman, D. *J. Phys. Chem B* (in press), and private communication.
56. Burley, S. K., and Petsko, G. A. (1988) *Adv. Protein Chem. 39*, 125−189.
57. Laberge, M. (1998) *Biochim. Biophys. Acta 1386*, 305−330.
58. Rodriguez-Lopez, J. N., Smith, A. T., and Thorneley, R. N. F. (1996) *J. Biol. Chem. 271*, 4023−4030.
59. Smulevich, G. (1995) *Biochem. Soc. Trans. 23*, 240−244.
60. Harvey, S. C. (1989) *Proteins: Struct., Funct., Genet. 5*, 78−92.
61. Sharp, K. A., and Honig, B. (1990) *Annu. Rev. Biophys. Biophys. Chem. 19*, 301−332.
62. Swartz, P. D., and Ichiye, T. (1997) *Biophys. J. 73*, 2733−2741.
63. Laberge, M., Gallantai, R., Schay, G., and Fidy, J. (2001) *Biophys. J. 80*, A1679.


BI002938A